Holographic study of reflected entropy in anisotropic theories

Mohammad Javad Vasli,[1,*] M. Reza Mohammadi Mozaffar,[1,†]
Komeil Babaei Velni,[1,‡] and Mohammad Sahraei[1,2,§]

[1]*Department of Physics, University of Guilan, P.O. Box 41335-1914, Rasht, Iran*
[2]*School of Particles and Accelerators, Institute for Research in Fundamental Sciences (IPM), P.O. Box 19395-5531, Tehran, Iran*

(Received 14 August 2022; accepted 19 December 2022; published 19 January 2023)

We evaluate reflected entropy in certain anisotropic boundary theories dual to nonrelativistic geometries using holography. It is proposed that this quantity is proportional to the minimal area of the entanglement wedge cross section. Using this prescription, we study in detail the effect of anisotropy on reflected entropy and other holographic entanglement measures. In particular, we study the discontinuous phase transition of this quantity for a symmetric configuration consisting of two disjoint strips. We find that in the specific regimes of the parameter space the critical separation is an increasing function of the anisotropy parameter and hence the correlation between the subregions becomes more pronounced. We carefully examine how these results are consistent with the behavior of other correlation measures including the mutual information. Finally, we show that the structure of the universal terms of entanglement entropy is corrected depending on the orientation of the entangling region with respect to the anisotropic direction.

DOI: 10.1103/PhysRevD.107.026012

I. INTRODUCTION

In recent years, the holographic framework allows us to quantitatively study the fascinating connections between quantum information and quantum gravity. In this context, different quantum information measures and their holographic counterparts have proved very useful for developing our understanding of the gauge/gravity correspondence, e.g., entanglement entropy and computational complexity [1,2]. In particular, the Ryu-Takayanagi (RT) prescription has proven immensely useful for investigating this connection in a robust manner, by constructing a geometrical realization of the entanglement entropy (EE) for a spatial subregion in the boundary field theory. Let us recall that EE has emerged as an interesting theoretical quantity which provides new insights into a variety of topics in physics ranging from quantum information theory to high energy physics (see [3,4] for reviews). Moreover, the entanglement entropy is the unique quantity which measures the amount of quantum entanglement between two subsystems for a given pure state. In this case, assuming that the total Hilbert space takes a direct product form of two Hilbert spaces of the subsystems, i.e., $\mathcal{H}=\mathcal{H}_A\otimes\mathcal{H}_{\bar{A}}$, the corresponding EE of the subsystem A is given as follows

$$S_A=-\mathrm{Tr}_A\rho_A\log\rho_A, \tag{1.1}$$

where ρ_A is the reduced density matrix defined as $\rho_A=\mathrm{Tr}_{\bar{A}}|\psi\rangle\langle\psi|$ and $|\psi\rangle$ denotes the corresponding pure state. The holographic counterpart of Eq. (1.1) can be obtained using RT prescription which states that EE is dual to the area of a minimal codimension-two bulk hypersurface Γ_A which is homologous to the boundary region A, i.e., [1]

$$S_A=\frac{\min\left(\mathrm{area}\,\Gamma_A\right)}{4G_N}. \tag{1.2}$$

Hence, in strongly coupled quantum field theories with holographic duals, computing EE reduces to a geometric problem of finding minimal hypersurfaces satisfying suitable boundary conditions. This proposal has stimulated a wide variety of research efforts investigating the properties and applications of holographic entanglement entropy (HEE), e.g., see [5,6] for reviews.

Further, EE fails to be a good measure of quantum entanglement or correlations between the subsystems for mixed states. A variety of correlation measures for such classes of states have been developed, e.g., logarithmic negativity [7], entanglement of purification [8], odd entropy [9] and reflected entropy [10]. Much of our analysis

*vasli@phd.guilan.ac.ir
†mmohammadi@guilan.ac.ir
‡babaeivelni@guilan.ac.ir
§msahraei@ipm.ir

in this paper will focus on studying reflected entropy in specific holographic settings, so we proceed by reviewing its definition. Consider a mixed state $\rho = \sum_i p_i |\rho_i\rangle\langle\rho_i|$ in $\mathcal{H}_A \otimes \mathcal{H}_B$. The canonical purification is defined on a doubled Hilbert space $\mathcal{H}_A \otimes \mathcal{H}_{A'} \otimes \mathcal{H}_B \otimes \mathcal{H}_{B'}$ and is given by

$$|\sqrt{\rho}\rangle = \sum_i \sqrt{p_i}\,|\rho_i\rangle \otimes |\rho_i\rangle. \tag{1.3}$$

Now the reflected entropy is the corresponding EE of the subsystem AA', i.e.,

$$S_R(A,B) = -\mathrm{Tr}\rho_{AA'} \log \rho_{AA'}, \tag{1.4}$$

where $\rho_{AA'} = \mathrm{Tr}_{BB'}|\sqrt{\rho}\rangle\langle\sqrt{\rho}|$. Clearly, the above definition reduces to EE when ρ is pure. There are several interesting inequalities which the reflected entropy satisfies generally, e.g.,

$$I(A,B) \le S_R(A,B) \le 2\ \min\{S_A, S_B\},$$
$$I(A,B) + I(A,C) \le S_R(A, B\cup C), \tag{1.5}$$

where $I(A,B)$ is the mutual information between A and B given as follows

$$I(A,B) = S_A + S_B - S_{A\cup B}. \tag{1.6}$$

In [10] the authors provided an interesting holographic interpretation of the canonical purification and also proposed a dual counterpart for the reflected entropy which is the minimal cross sectional area of the entanglement wedge. Before we proceed further, let us recall that the entanglement wedge is the bulk region corresponding to the reduced density matrix ρ_A and whose boundary is $A \cup \Gamma_A$. Considering a spatial boundary region consists of two disjoint parts A and B and denoting the cross sectional area of the entanglement wedge by $\Sigma_{A\cup B}$ the corresponding reflected entropy is given by

$$S_R(A,B) = \frac{\min\,(\mathrm{area}\,\Sigma_{A\cup B})}{2G_N}. \tag{1.7}$$

A key feature of the above proposal is that the holographic reflected entropy presents a discontinuous phase transition from zero to positive values as the two subregions get closer. This transition is due to the competition between a connected and a disconnected configuration for the entanglement wedge. Indeed, for large separations where the disconnected configuration is favored, $\Sigma_{A\cup B}$ becomes empty and the corresponding reflected entropy vanishes. Let us recall that there exist other measures which seem to be dual to entanglement wedge cross section (EWCS). These proposals can be summarized as follows [9–11]

$$E_W(A,B) = \frac{S_R(A,B)}{2} = \frac{\mathcal{E}(A,B)}{\chi_d} = S_O(A,B) - S(A\cup B), \tag{1.8}$$

where S_R, $\mathcal{E}$ and S_O are reflected entropy, logarithmic negativity and odd entropy respectively. Here χ_d is a constant which depends on the dimension of the spacetime. These proposals has since been the subject of a large body of work [11–31]. Further, a wide variety of recent research efforts investigating the properties of the corresponding measures from the perspective of the boundary theory have also appeared in [32–41].

Our goal in this paper is to present another step in this research program, in which we investigate the behavior of reflected entropy in anisotropic systems with strong interactions by means of holography. Let us recall that anisotropic holographic models have already been extensively studied in the context of AdS/QCD to scan the QCD phase diagram and also to investigate different aspects of quark-gluon plasma which is produced in relativistic heavy ion collisions, e.g., [42–48]. On the other hand, in the context of AdS/CMT, anisotropic holographic models appear in many examples of quantum criticality in condensed matter physics with nonrelativistic fixed points [49,50]. Further, some investigations attempting to better understand the behavior of different holographic entanglement measures in anisotropic backgrounds have also appeared in [51–56]. In this paper, we aim to provide a detailed study of the influence of anisotropy on the behavior of reflected entropy. An especially interesting question concerns how the phase transition of this quantity is affected by anisotropy. We will also discuss how our results are comparable with the behavior of other correlation measures including the holographic mutual information (HMI).

The remainder of our paper is organized as follows: In Sec. II, we give the general framework in which we are working, establishing our notation and the general form of the HEE and reflected entropy functionals in a static anisotropic background. In Sec. III, we consider an anisotropic geometry whose dual state exhibits an specific phase transition which is similar to confinement-deconfinement and study the properties of reflected entropy numerically. To get a better understanding of the results, we will also compare the behavior of reflected entropy to other correlation measures including HEE and HMI. In Sec. IV, we extend our studies to a family of axion-dilaton gravity theories underlying solution breaks isotropy while preserving translation invariance. By tuning the dilaton potential, we study the influence of anisotropy on reflected entropy in different backgrounds. In the latter case we present a combination of numerical and analytic results on the scaling of different correlation measures. Next, we study a specific geometry with anisotropic Lifshitz scale invariance in Sec. V. We review our main results and discuss their physical implications in Sec. VI, where we also indicate some future directions.

II. SETUP

In this section, we briefly review some preliminaries to construct the holographic reflected entropy functional in generic anisotropic geometries. We focus our analysis on the special case of a five-dimensional bulk geometry because the interesting qualitative features of the reflected entropy are independent of the dimensionality of the boundary field theory. In this case, the general form of an anisotropic background can be written as[1]

$$ds^2 = \frac{R^2}{r^2} H(r) \left(-f(r) b(r) dt^2 + \sum_{n=1}^{3} G_n(r) dx_n^2 + \frac{dr^2}{f(r)} \right), \tag{2.1}$$

where R is the curvature radius. Without loss of generality, we will from now on consider $R = 1$. In order to investigate the effect of anisotropy on the reflected entropy we consider the simplest boundary entangling region consisting of two disjoint long narrow strips with equal width ℓ separated by h on a constant time slice (see Fig. 1). Further, to examine the effects of changing the direction of the strip, we lay entangling region in some arbitrary direction using rotation with Euler angles as follows

$$x_i(\xi) = \sum_{j=1,2,3} a_{ij}(\alpha, \beta, \gamma) \xi_j, \quad i = 1, 2, 3 \tag{2.2}$$

where a_{ij} is the entry of the rotation matrix and α, β, and γ denote the angles of rotation around x, y, and z directions, respectively. For simplicity, we will only consider rotations around the y-axis. Considering the width of the strip along the ξ_1 direction and using Eq. (2.1), the entropy functional is then given by the following expression

$$S = \frac{L^2}{4G_N} \int \frac{H^{\frac{3}{2}}(r)}{r^3} \sqrt{\mathcal{G}(r) \xi_1'^2 + \frac{\mathcal{T}(r,\beta)}{f(r)}} dr, \tag{2.3}$$

where the prime indicates derivative with respect to r and we have defined

$$\mathcal{T}(r,\beta) = G_2(r)(G_1(r)\sin^2\beta + G_3(r)\cos^2\beta),$$
$$\mathcal{G}(r) = G_1(r) G_2(r) G_3(r). \tag{2.4}$$

Further, using the equation of motion, the width of the entangling region and HEE can be written as follows

[1]Note that using the reparameterization invariance one can fix $G_1(r)$ and $G_2(r)$ in Eq. (2.1) and once this is done, $b(r)$ cannot be set to unity in general. In Sec. IV B we consider a specific background with $b(r) \neq 1$.

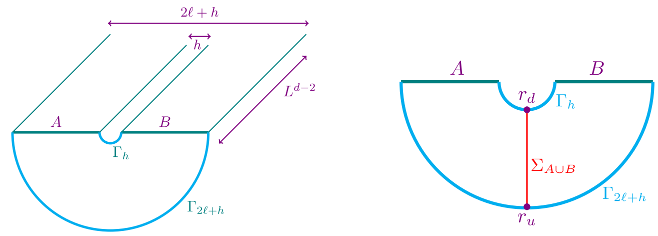

FIG. 1. Left: schematic minimal hypersurfaces for computing $S_{A\cup B}$ in connected configuration. Right: the minimal cross section of the entanglement wedge, Σ in red. Here we only show the connected configuration where the reflected entropy is nonzero.

$$\ell = 2 \int_0^{r_t} \frac{\sqrt{\mathcal{T}(r,\beta)}}{\sqrt{f(r)\mathcal{G}(r)} \sqrt{\frac{r_t^6}{r^6} \frac{\mathcal{G}(r) H(r)^3}{\mathcal{G}(r_t) H(r_t)^3} - 1}} dr. \tag{2.5}$$

$$S = \frac{L^2}{2G_N} \int_\epsilon^{r_t} \frac{r_t{}^3 \sqrt{\mathcal{G}(r)} H(r)^3}{r^3 \sqrt{f(r)}} \times \sqrt{\frac{\mathcal{T}(r,\beta)}{r_t{}^6 \mathcal{G}(r) H(r)^3 - r^6 \mathcal{G}(r_t) H(r_t)^3}} dr, \tag{2.6}$$

where r_t denotes the turning point of the minimal hypersurface and we regulate the calculation of the entropy in the standard way by introducing a cutoff surface at $r = \epsilon$.

Let us now turn to the computation of the reflected entropy in this setup using Eq. (1.7). Due to the symmetry of the configuration that we have chosen, $\Sigma_{A\cup B}$, lies entirely on $\xi_1 = 0$ slice and as a consequence, from Eq. (2.1), we find the reflected entropy to be

$$S_R = \frac{L^2}{2G_N} \int_{r_d}^{r_u} \frac{H^{\frac{3}{2}}(r)}{r^3} \sqrt{\frac{\mathcal{T}(r,\beta)}{f(r)}} dr, \tag{2.7}$$

where r_d and r_u denote the corresponding turning points of Γ_h and $\Gamma_{2\ell+h}$ respectively (see Fig. 1).

III. EINSTEIN-DILATON-TWO-MAXWELL THEORIES

The first model we consider is that of an anisotropic background in Einstein-dilaton-two-Maxwell Theories. The corresponding metric is given as follows [57]

$$ds^2 = \frac{e^{-\frac{r^2}{2}}}{r^2} \left(-f(r) dt^2 + \frac{dr^2}{f(r)} + dx^2 + r^{2-\frac{2}{\nu}} (dy^2 + dz^2) \right). \tag{3.1}$$

The explicit forms of $f(r)$ is tedious and hence we do not explicitly show the corresponding expressions here. Clearly, the strength of the anisotropy between boundary spatial directions is parametrized by ν and for $\nu = 1$ we have a isotropic background. This metric is a solution to

Einstein gravity coupled to a dilaton and two Maxwell fields with a nontrivial scalar potential. In comparing the above expression with metric (2.1), we should identify

$$G_1(r)=1, \quad G_2(r)=G_3(r)=r^{2-\frac{2}{\nu}}, \quad H(r)=e^{-\frac{r^2}{2}}. \tag{3.2}$$

The corresponding expression for HEE and reflected entropy can be obtained using Eqs. (2.6) and (2.7) and the above identifications. Different aspects of HEE in the dual boundary theory have been studied in [54]. Before we proceed further, let us comment on a characteristic property of this geometry. Indeed, as demonstrated in [54], for some values of r_h we can find several HEE for same value of ℓ, and based on (1.2), We have to choose the smallest ones. The transition between different hypersurfaces shows itself as a phase transition on HEE which gives some things very similar to crossover transition between confinement-deconfinement phases in the dual gauge theory. Further, the thermodynamical properties of this gravitational background were studied in [57] and it was shown that it has a Van der Waals-like phase transition between small and large black holes for a specific range of the boundary chemical potential. More explicitly, the thermal entropy function is multivalued for $0<\mu<\mu_{\mathrm{crit.}}(\nu)$ and becomes one-to-one for $\mu_{\mathrm{crit.}}(\nu)<\mu$. Let us mention that in the large black hole phase, the connected surface is always smaller than the disconnected surface and the phase transition similar to [53] does not happen. On the other hand, in the small black hole phase, HEE becomes multivalued and a phase transition happens. This transition is different from the phase transition in [53] and cannot realize as a confinement-deconfinement phase transition. In the next subsections we will compute the holographic entanglement measures numerically and treat these cases separately.

A. Reflected entropy for the large black hole

In this case we choose μ such that we have Van der Waals-like phase transition. We also set $r_h=1$ throughout this section and hence we are in large black hole phase. Also for simplicity, we have rescaled the holographic measures, i.e., $\{S,I\}\rightarrow\frac{4G_N}{L^2}\{S,I\}$ and $S_R\rightarrow\frac{2G_N}{L^2}S_R$.

In Fig. 2 we show the dependence of the HEE, HMI and reflected entropy for specific values of ν as a function of the rotation angle with $\ell=0.4$ and $h=0.2$. The dashed curve corresponds to isotropic case with $\nu=1$ where the measures are independent of the rotation angle. The left panel demonstrates the dependence of the finite part of the HEE defined as $\Delta S\equiv S-S_{\mathrm{dis}}$ on β. Here S_{dis} is the area of two disconnected straight lines extending from the endpoints of the boundary line segment to horizon of black hole. Note that based on this definition the disconnected piece depends on the temperature. The corresponding area functional can be obtained by setting $\xi_1'=0$ in Eq. (2.3)

$$S_{\mathrm{dis}}=\frac{L^2}{2G_N}\int_0^{r_h}\frac{H^{\frac{3}{2}}(r)}{r^3}\sqrt{\frac{\mathcal{T}(r,\beta)}{f(r)}}dr. \tag{3.3}$$

We see that I and S_R have a maximum at $\beta=\pi/2$ where the HEE develops a minimum. This minimum becomes deeper and sharper for larger values of ν.

We present the dependence of the turning point and the corresponding HEE and HMI for specific values of β as a function of the width of the subregions and separation between them with $\nu=2$ in Fig. 3. Again, the dashed curve corresponds to isotropic case with $\nu=1$. The left panel shows that for a fixed boundary width, as ν increases from 1, r_t decreases which means that the bulk potential due to the anisotropy pushes the minimal hypersurface towards the boundary. This behavior is enhanced by increasing the rotation angle from 0 to $\frac{\pi}{2}$. The right panel shows the HMI as a function of the dimensionless boundary quantity h/ℓ. Based on these plots for fixed ν we observe that although the HEE decreases with the rotation angle, the HMI increases with β. This result holds for any value in the range $0\leq\beta\leq\pi/2$. We must point out that in this metric the connected surface for HEE is always smaller than the disconnected surface and as a result, the phase transition similar to [58] does not happen. Also the disconnected surface here is a U shape surface which consists of two parts, a term coming from Eq. (2.3) and another term corresponds to a surface which lies on the horizon of the black hole.

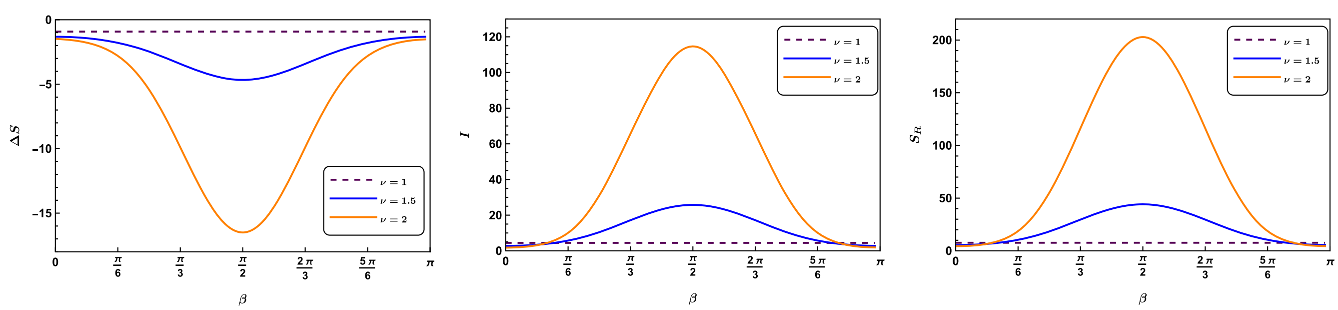

FIG. 2. Finite part of the HEE (left), HMI (middle), and reflected entropy (right) as a function of rotation angle for different values of ν with $\ell=0.4$ and $h=0.2$. The dashed curve corresponds to isotropic case with $\nu=1$ where the measures are independent of the rotation angle.

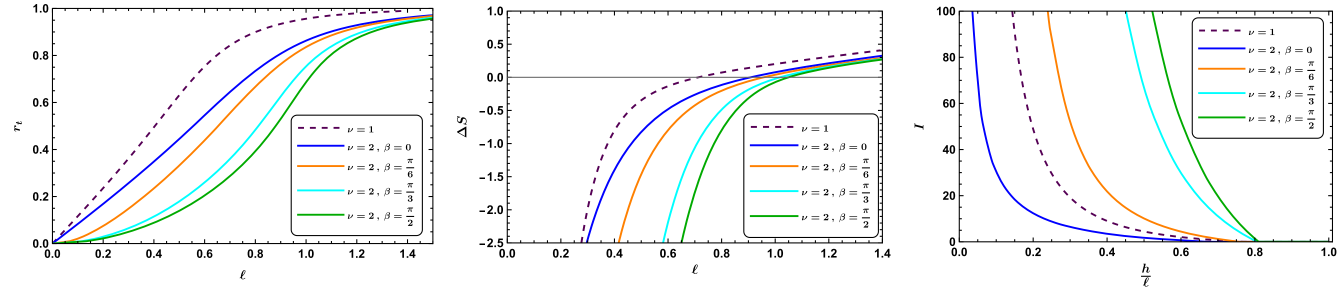

FIG. 3. Left: the turning point of the RT hypersurface as a function of the width of the boundary subregion for different values of the rotation angle. Middle: the HEE as a function of ℓ for the same values of β. Right: the HMI as a function of $\frac{h}{\ell}$. The solid curves show the anisotropic case with $\nu = 2$ and the dashed curve corresponds to isotropic case with $\nu = 1$.

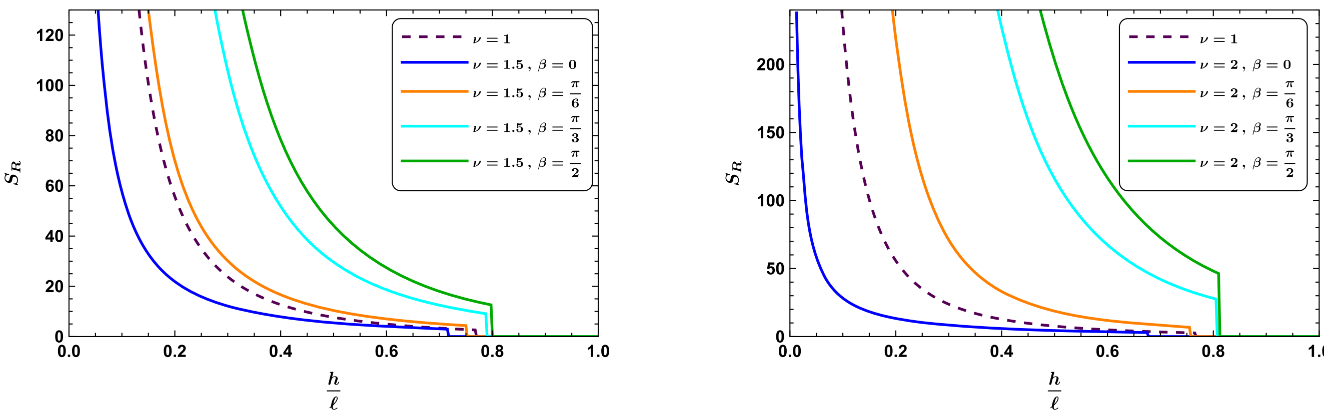

FIG. 4. Reflected entropy as a function of $\frac{h}{\ell}$ for different values of β with $\nu = 1.5$ (left) and $\nu = 2$ (right). In both plots the dashed curve corresponds to isotropic case with $\nu = 1$. Here we set $\ell = 0.4$.

Figure 4 shows the reflected entropy as a function of h/ℓ for different values of ν and β. Let us make a number of observations regarding these numerical results. First, we note that in both plots, in the aforementioned range of the rotation angle, the reflected entropy increases with β. Next, the phase transition of this measure happens at larger separations between the two subregions comparing to $\beta = 0$ case. Hence regarding the reflected entropy as a measure of total correlation between the two subregions, we see that decreasing the rotation angle promotes disentangling between them. Moreover, despite the $\beta = 0$ case where the critical separation decreases with ν, for other values of the rotation angles, $(\frac{h}{\ell})_{\text{crit}.}$ increases with this parameter. In Fig. 5 we present the critical separation as a function of ν to allow for a meaningful comparison between the different cases. We see that $(\frac{h}{\ell})_{\text{crit}.}$ becomes a monotonically increasing function of ν for large values of the rotation angle. For example, if we choose $\beta = \pi/2$, then increasing the anisotropy, the critical separation increases which means that the correlation between the subregions becomes stronger. Also for intermediate values of β, e.g., $\beta = \pi/6$, the critical separation has a minimum at $\nu \sim 1.5$.

B. Reflected entropy for the small black hole

As we have mentioned before, in this geometry the free energy is multivalued and the background exhibits a Van der Waals-like phase transition between small and large black holes. As explained in [57] for $\mu < \mu_{\text{crit}.}$ the curves

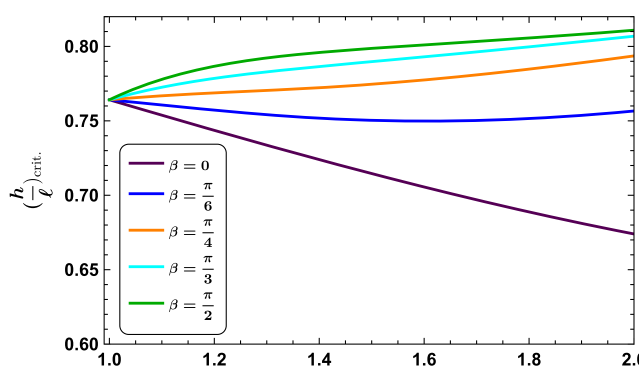

FIG. 5. Critical separation between the subregions as a function of ν for different values of β. For large values of the rotation angle the critical separation is an increasing function of ν and hence the correlation between the subregions becomes stronger.

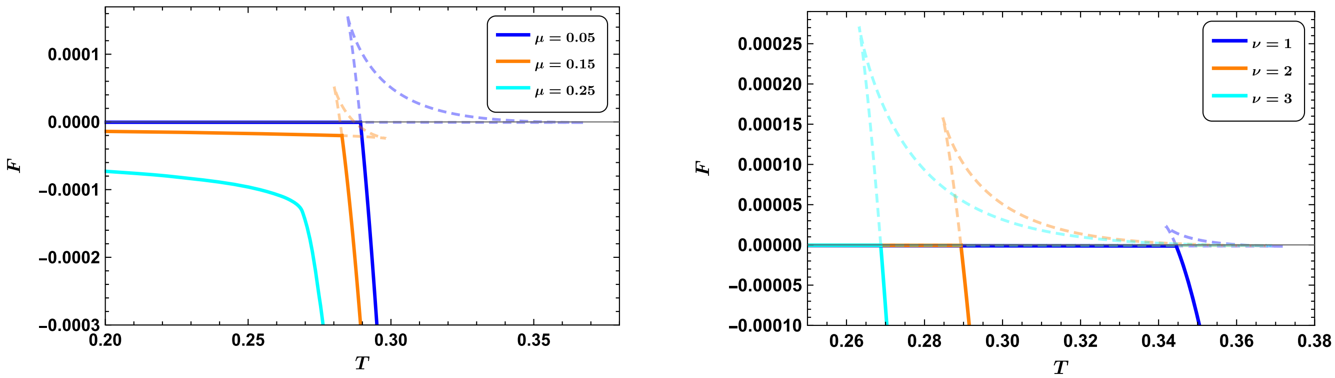

FIG. 6. The free energy as a function of temperature for different values of the chemical potential with $\nu = 2$ (left) and different values of the anisotropy parameter with $\mu = 0.05$ (right). The dashed region indicates the instability zone and the point where any curve intersects itself corresponds to the small/large black holes phase transition. Here we set $\ell = 0.4$.

for $F(T)$ form a swallow tail shape such that an increase in μ give a decrease in size for the swallow tail region, e.g., see the left panel in Fig. 6. In the right panel we show the same function for different values of the anisotropy parameter with $\mu = 0.05$. Interestingly, we see that in this case an increase in ν give an increase in size for the swallow tail region. We set $r_h = 3.7$ throughout this section and hence we are in the small black hole phase. In the case of small black hole, HEE is multivalued and we must choose the minimum configuration. This phase transition cannot be realized as a common confinement/deconfinement phase transition which first investigated in [58]. This difference comes from the fact that the connected surface is always dominant and hence no connected/disconnected phase transition happens. Hence, the entanglement entropy is always of order $\mathcal{O}(N^2)$ for any subsystem size [53].

Figure 7 shows the turning point of the RT hypersurface and the HEE as a function of width of subregion for $\nu = 2$ and different values of β. As mentioned above, HEE is multivalued for some width of the subregion and we must choose the minimum configuration. Figure 8 shows the HMI and the reflected entropy as a function of $\frac{h}{\ell}$ for $\nu = 2$ and different values of β. The general behavior of these two measures is very similar to the large black hole phase, but in this case they also exhibit a phase transition. As can be seen in the inset, due to HEE phase transition, there is a discontinuity in the HMI and the reflected entropy.

IV. ANISOTROPIC EINSTEIN-AXION-DILATON GRAVITIES

In this section we evaluate reflected entropy and some other holographic entanglement measures for an anisotropic geometry in a family of axion-dilaton gravity theories with the following action [59–61]

$$I = \frac{1}{16\pi G_N}\int d^5x\sqrt{-g}\left(R - \frac{1}{2}(\partial\phi)^2 + V(\phi) - \frac{1}{2}Z(\phi)(\partial\chi)^2\right). \tag{4.1}$$

Here $V(\phi)$ is the dilaton potential and $Z(\phi)$ controls the strength of the coupling between the dilaton and the axion field. As noted in [61], assuming a linear axion ansatz, i.e., $\chi = az$, the equations of motion automatically satisfied

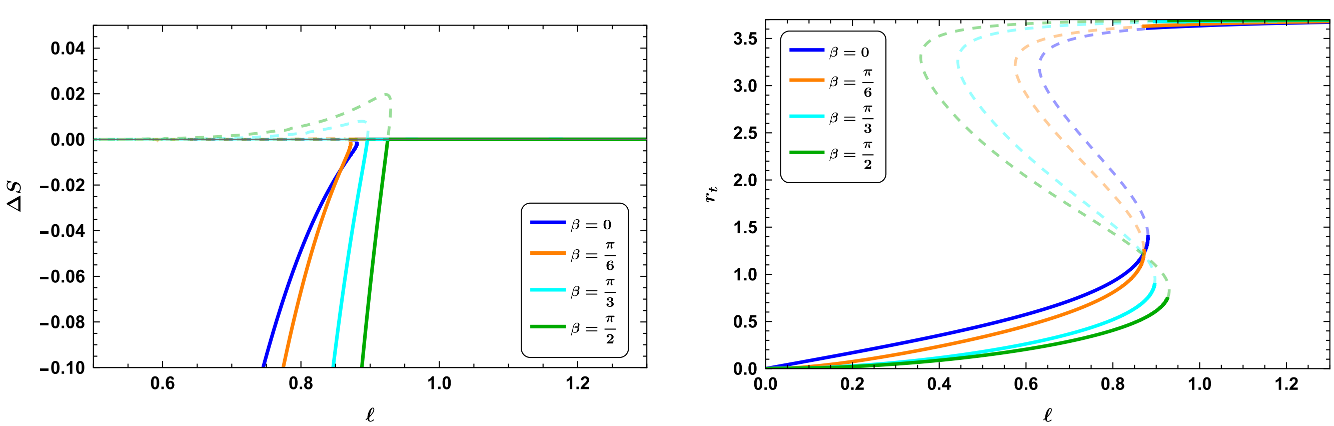

FIG. 7. The HEE (left) and the turning point of the RT hypersurface (right) as functions of ℓ for different values of β. Here we set $\nu = 2$ and the dashed part of each curve corresponds to the parametric region where the HEE becomes multivalued.

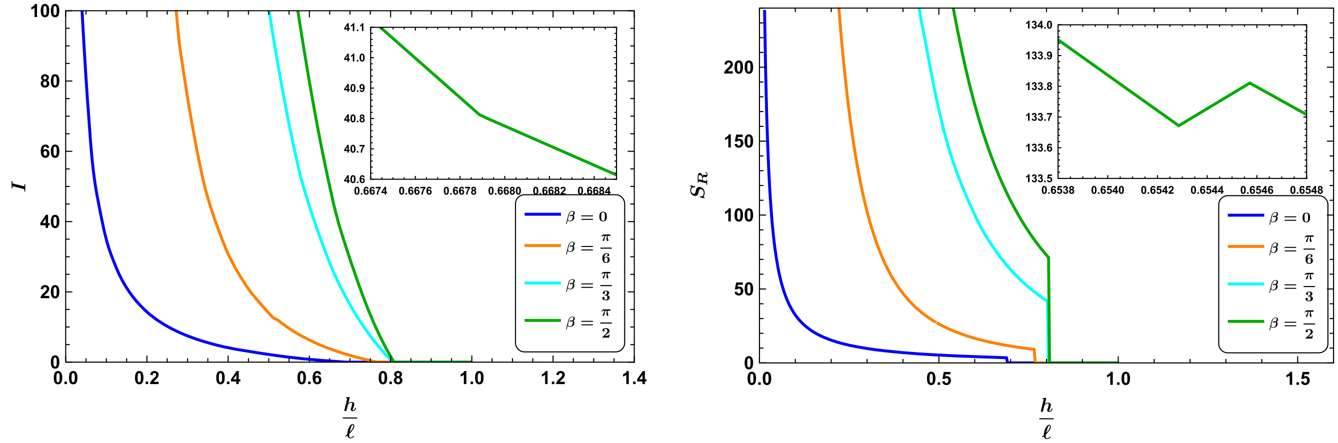

FIG. 8. The HMI (left) and reflected entropy (right) as functions of $\frac{h}{\ell}$. Right: reflected entropy as a function of $\frac{h}{\ell}$. Here we set $\nu = 2$ and $\ell = 0.35$. The discontinuity depicted in the inset corresponds to the region where the HEE becomes multivalued.

such that the underlying geometry breaks isotropy while preserving translation invariance

$$ds^2 = e^{2A(r)}\left(-f(r)dt^2 + dx^2 + dy^2 + e^{2g(r)}dz^2 + \frac{dr^2}{f(r)}\right),$$
$$\phi = \phi(r). \tag{4.2}$$

The above metric is asymptotically AdS near $r = 0$ and $g(r)$ controls the degree of anisotropy between spatial directions. Let us add that, for $V = 12$ and $Z = e^{2\phi}$ the dual field theory is conformal. Moreover, a confining boundary theory can be obtained by considering specific dependence for these functions. For instance, choosing

$$V(\phi) = 12\cosh(\sigma\phi) + b\phi^2, \qquad Z(\phi) = e^{2\gamma\phi}, \tag{4.3}$$

with $b \equiv \frac{\Delta(4-\Delta)}{2} - 6\sigma^2$, the corresponding boundary theory has a confined phase for $\sigma \geq \sqrt{2/3}$ [62]. Here Δ is the scaling dimension of the scalar operator dual to ϕ. In the following, we study influence of anisotropy on holographic information measures in different backgrounds.

A. Nonconformal boundary theory

In this case we consider a marginal scalar operator with $\Delta = 4$ at zero temperature, i.e, $f(r) = 1$. A perturbative solution for the equations of motion in the small anisotropy limit was found in [63] where the metric is given by (4.2) with

$$A(r) = -\log(r) - \frac{a^2r^2}{72} + \frac{a^4r^4}{1200}(3\gamma^2+1)(1-5\log(ar)) + \mathcal{O}(ar)^6, \tag{4.4}$$

$$g(r) = \frac{a^2r^2}{8} - \frac{a^4r^4}{2592}(31+81\gamma^2-54(3\gamma^2+1)\log(ar)) + \mathcal{O}(ar)^6. \tag{4.5}$$

Let us mention that in this background, the xy plane is isotropic and hence the rotation of the strip around the z axis has no effect on holographic correlation measures. Further, in comparing (4.2) with metric (2.1), we should identify

$$H(r) = r^2e^{2A(r)}, \quad G_1(r) = G_2(r) = 1, \quad G_3(r) = e^{2g(r)}, \tag{4.6}$$

and thus

$$\mathcal{G} = e^{2g(r)}, \qquad \mathcal{T}(r,\beta) = \sin^2\beta + e^{2g(r)}\cos^2\beta. \tag{4.7}$$

The corresponding expression for HEE and reflected entropy can be obtained using Eqs. (2.6) and (2.7) and the above identifications. In the following, we first provide a numerical analysis and examine the dependence of different measures on the anisotropy parameter. Next, we carry out a perturbative analysis for calculating these measures in the specific regimes of the parameter space.

1. Numerical results

In Fig. 9 we show the turning point of the RT hypersurface and HEE as functions of the rotation angle for different values of the anisotropy parameter for a fixed extent of the boundary subregion. The left panel shows that in a specific range of the rotation angle, i.e., $\frac{\pi}{6} \lesssim \beta \lesssim \frac{5\pi}{6}$, increasing the anisotropy, the RT hypersurfaces reach deeper into the bulk, so they carry more information about the geometry. Notice that validity of the background solution was assumed and we set the subleading terms in Eq. (4.4) to zero. This asymptotic behavior is valid for $ar_t \ll 1$, or equivalently, $a\ell \ll 1$, the range of anisotropy that we shall consider in the following. The right panel illustrates the HEE, which is regularized by subtracting the divergent part of Eq. (2.6). This divergent term up to the order a^2 correction becomes

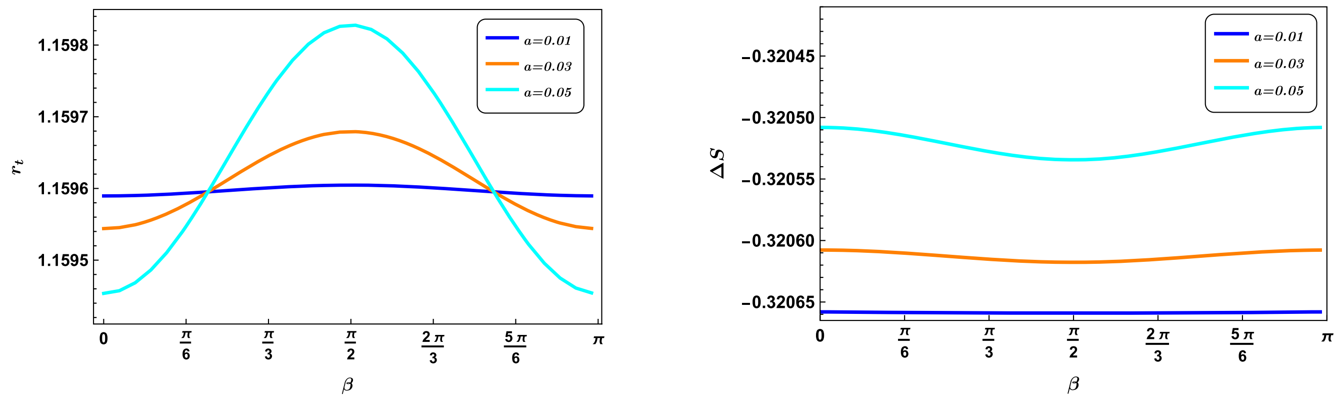

FIG. 9. The turning point of the RT hypersurface (left) and HEE (right) as functions of the rotation angle for different values of the anisotropy parameter. Here we set $\ell = 1$.

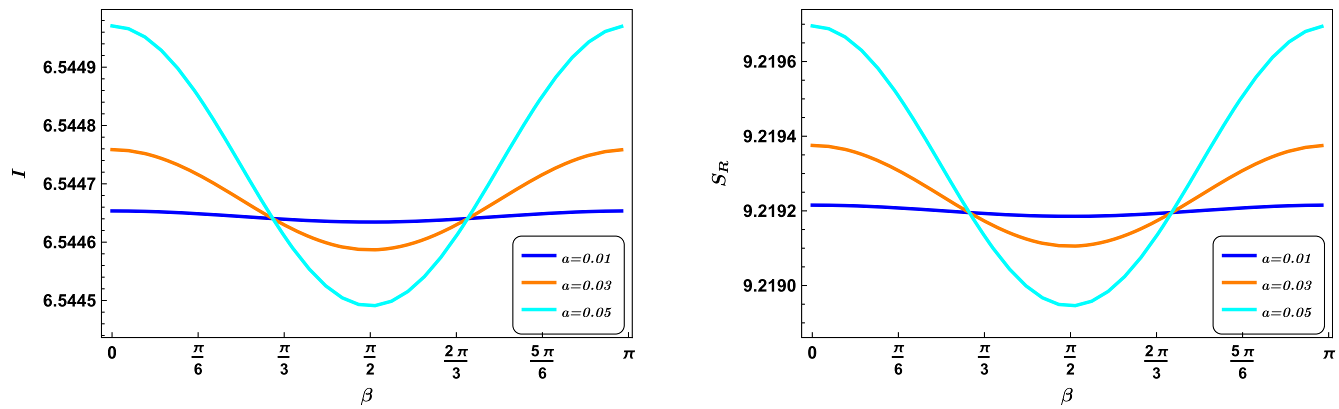

FIG. 10. HMI (left) and reflected entropy (right) as functions of β for $\ell = 1$, $h = 0.2$ and different values of a.

$$S_{\rm div} = \frac{1}{2G_N}\left(\frac{1}{\epsilon^2} - \frac{1}{24}a^2(1+3\cos(2\beta))\log\epsilon\right). \qquad (4.8)$$

In Fig. 10 we show the HMI and reflected entropy as functions of β for different values of a and specific values of ℓ and h. Clearly the qualitative behavior of these two measures is similar as expected. As we mentioned before both the HMI and reflected entropy are measures of total correlation between subregions, hence the holographic calculations reproduce the expected behavior. Moreover, based on these figures, the corresponding correlations develop a minimum at $\beta = \pi/2$. In Fig. 11, we show the phase transition point of reflected entropy as a function of the rotation angle. Interestingly, we see that for $\frac{\pi}{6} \lesssim \beta \lesssim \frac{5\pi}{6}$, increasing the anisotropy, the critical separation increases which means that the correlation between the subregions becomes stronger. We will confirm these observations as well as some new results with a perturbative analysis below.

2. Perturbative treatment

As we mentioned before in $a\ell \ll 1$ limit the metric (4.2) is a small deformation of pure AdS, thus we can use a perturbative expansion to compute the variation of holographic information measures. To do so, we can perform a change of variables in the corresponding expressions for ℓ, S and S_R to the dimensionless coordinate $u = \frac{r}{r_t}$.

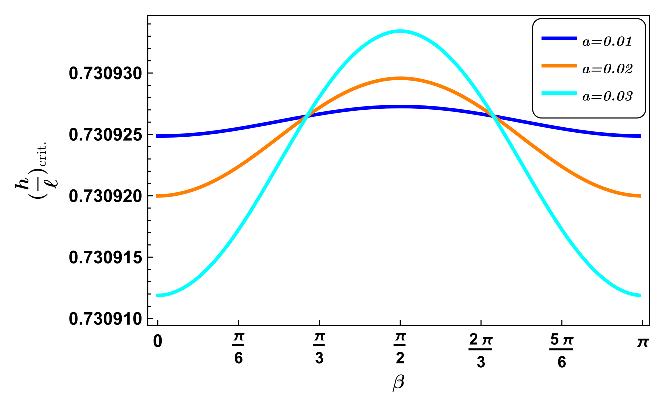

FIG. 11. Critical separation between the subregions as a function of β for different values of a. For $\beta \sim \pi/2$ of the rotation angle the critical separation is an increasing function of the anisotropy parameter and hence the correlation between the subregions becomes stronger.

In this situation, the corresponding boundary quantities become

$$\ell = 2r_t \int_0^1 \frac{\sqrt{\mathcal{T}(u,\beta)}}{e^{g(u)}\sqrt{\frac{e^{2g(u)}e^{6A(u)}}{e^{2g(1)}e^{6A(1)}} - 1}} du, \tag{4.9}$$

$$S = \frac{L^2 r_t}{2G_N} \int_{\epsilon/r_t}^1 \frac{e^{g(u)}e^{6A(u)}\sqrt{\mathcal{T}(u,\beta)}}{\sqrt{e^{2g(u)}e^{6A(u)} - e^{2g(1)}e^{6A(1)}}} du, \tag{4.10}$$

$$S_R = \frac{L^2 r_t}{2G_N} \int_{r_d/r_t}^{r_u/r_t} e^{3A(u)}\sqrt{\mathcal{T}(u,\beta)} du. \tag{4.11}$$

Now we expand Eq. (4.9) in the limit $a\ell \ll 1$ to find the leading corrections to r_t compared to its pure AdS value. Note that in this case the corresponding turning point is close to the boundary, i.e., $ar_t \ll 1$. In this limit Eq. (4.9) can be written in terms of the following expansion

$$\begin{aligned}\ell = {}& 2r_t \int_0^1 \frac{u^3}{\sqrt{1-u^6}} du \\ & + 2r_t^3 a^2 \int_0^1 \frac{(2\cos^2(\beta) - (3(u^6+u^4+u^2)-2)\sin^2(\beta))}{24\sqrt{\frac{1}{u^6}-1}(u^4+u^2+1)} du.\end{aligned} \tag{4.12}$$

The above integral can be evaluated explicitly yielding

$$\ell = 2r_t(c + a^2 r_t^2 \mathcal{C}_1(\beta)), \tag{4.13}$$

where

$$c = \frac{\sqrt{\pi}\Gamma(\frac{2}{3})}{\Gamma(\frac{1}{6})}, \quad \mathcal{C}_1(\beta) = -0.005 + 0.021\cos 2\beta. \tag{4.14}$$

Notice that the first term in Eq. (4.13) is the pure AdS contribution. Inverting this equation, we can represent the turning point as a function of ℓ

$$r_t = \frac{\ell}{2c}\left(1 - a^2\ell^2 \frac{\mathcal{C}_1(\beta)}{4c^3}\right). \tag{4.15}$$

Let us comment on the properties of the above result: First, we observe that the location of the turning point is unaffected for $\beta_1 \sim 0.66$ (or equivalently $\beta_2 \sim \pi - 0.66$) where $\mathcal{C}_1(\beta_{1,2}) = 0$. Moreover, for $\beta_1 \leq \beta \leq \beta_2$, $\mathcal{C}_1(\beta)$ is negative and therefore the correction to r_t in Eq. (4.15) is positive. Hence the RT hypersurfaces can probe more of the bulk geometry due to the presence of anisotropy. These results are consistent with the previously numerical results illustrated in the left panel of Fig. 9.

Now we proceed to examine the leading correction to HEE from Eq. (4.10) using a similar reasoning to that above. Let us mention that it will be more convenient to separate the divergent piece in this integral. A simple analysis shows that in this case the HHE takes the following form

$$\begin{aligned}S = {}& \frac{1}{4G_N}\left(\frac{1}{\epsilon^2} - \frac{c}{r_t^2}\right) + \frac{1}{2G_N}a^2\left(\mathcal{C}_2(\beta)\log\frac{r_t}{\epsilon} + \mathcal{C}_3(\beta)\right) \\ & + \mathcal{O}(a^4),\end{aligned} \tag{4.16}$$

where

$$\begin{aligned}\mathcal{C}_2(\beta) &= \frac{1}{48}(1 + 3\cos 2\beta), \\ \mathcal{C}_3(\beta) &= 0.021 + 0.014\cos 2\beta.\end{aligned} \tag{4.17}$$

In principle then, we can invert the above expressions to write our result in terms of the width of the entangling region. Combining Eqs. (4.15) and (4.16), we obtain the first order correction to HEE as follows

$$\begin{aligned}S = {}& \frac{1}{4G_N}\left(\frac{1}{\epsilon^2} - \frac{4c^3}{\ell^2}\right) \\ & + \frac{1}{2G_N}a^2\left(\mathcal{C}_2(\beta)\log\frac{\ell}{2c\epsilon} - \mathcal{C}_1(\beta) + \mathcal{C}_3(\beta)\right).\end{aligned} \tag{4.18}$$

A key feature of the above result is the appearance of a new universal logarithmic term which depends on the anisotropy parameter. The coefficient of this term depends also on the rotation angle of the entangling region such that in the $\beta \sim 0.955$ limit where $\mathcal{C}_2(\beta) = 0$, vanishes. Roughly, we can think of this universal term as characterizing when the isotropy is broken in the underlying boundary theory. Similarly, as shown in [64], if instead we choose a background which breaks the translation invariance the structure of the universal terms of HEE is modified. Next, the HMI can be determined using Eqs. (1.6) and (4.18) as follows

$$\begin{aligned}I = {}& \frac{c^3}{G_N}\left(-\frac{2}{\ell^2} + \frac{1}{h^2} + \frac{1}{(2\ell+h)^2}\right) \\ & + \frac{1}{2G_N}a^2\mathcal{C}_2(\beta)\log\frac{\ell^2}{h(2\ell+h)}.\end{aligned} \tag{4.19}$$

Finally expanding Eq. (4.11) we can derive the following expression for the reflected entropy at leading order

$$S_R = \frac{1}{4G_N}\left(\frac{1}{r_d^2} - \frac{1}{r_u^2}\right) + \frac{1}{2G_N}a^2\mathcal{C}_2(\beta)\log\frac{r_u}{r_d}. \tag{4.20}$$

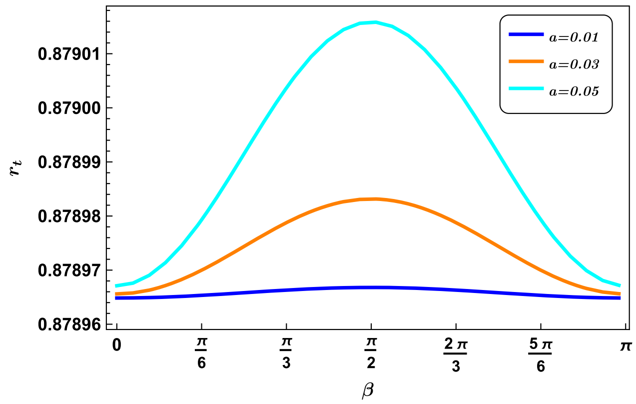

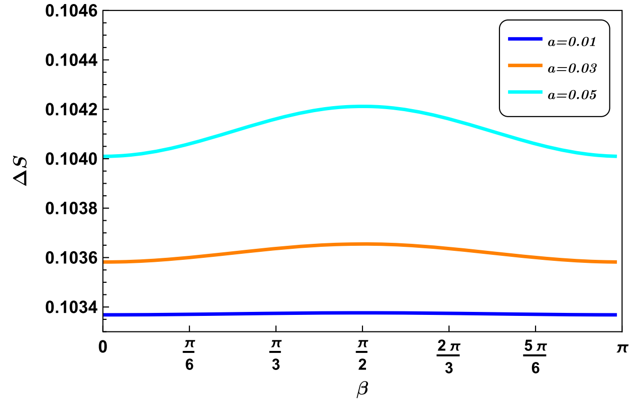

FIG. 12. The turning point of the RT hypersurface (left) and HEE (right) as functions of the rotation angle for different values of the anisotropy parameter. Here we set $\ell = 1$.

We can use Eq. (4.15) to rewrite the above result as follows

$$S_R = \frac{c^2}{G_N}\left(\frac{1}{h^2} - \frac{1}{(2\ell + h)^2}\right) + \frac{1}{2G_N} a^2 \mathcal{C}_2(\beta) \log\frac{2\ell + h}{h}. \tag{4.21}$$

Interestingly, we see that for $\mathcal{C}_2(\beta) = 0$, where the universal term vanishes, the reflected entropy is independent of the anisotropy parameter (see Fig. 10). In this case the corresponding transition point of the HMI and reflected entropy is independent of a which is consistent with the results presented in Fig. 11.

B. Strongly coupled anisotropic plasma

In this section we extend our analysis to another five-dimensional axion-dilaton-gravity theory which is dual to a strongly coupled anisotropic plasma at finite temperature. The corresponding action and dilaton potential are given by Eqs. (4.1) and (4.3) with $\sigma = 0$. Again, we consider a linear axion ansatz, i.e., $\chi = az$. As shown in [42], in high-temperature limit, it is possible to find analytic expressions for the metric as follows

$$ds^2 = \frac{e^{-\frac{\phi(r)}{2}}}{r^2}\left(-f(r)b(r)dt^2 + dx^2 + dy^2 + e^{-\phi(r)}dz^2 + \frac{dr^2}{f(r)}\right), \tag{4.22}$$

where

$$f(r) = 1 - \frac{r^4}{r_h^4} + \frac{a^2}{24 r_h^2}\left(8r^2(r_h^2 - r^2) - 10r^4 \log 2 + (3r_h^4 + 7r^4)\log\left(1 + \frac{r^2}{r_h^2}\right)\right), \tag{4.23}$$

$$b(r) = 1 - \frac{a^2 r_h^2}{24}\left(\frac{10r^2}{r_h^2 + r^2} + \log\left(1 + \frac{r^2}{r_h^2}\right)\right),$$
$$\phi(r) = -\frac{a^2 r_h^2}{4}\log\left(1 + \frac{r^2}{r_h^2}\right). \tag{4.24}$$

By high-temperature limit, we mean that $a \ll T$ which implies that $ar_h \ll 1$.

The corresponding analysis for evaluating the holographic measures follows similarly to the previous section, with the obvious replacement of the metric components in Eqs. (2.6) and (2.7). Unfortunately, it is not possible to compute the dependence of the measures on a perturbatively even for certain values of the rotation angle. Thus, in what follows we just present the numerical results. Let us add that a simple analysis shows that in this case the divergent term of the HEE is the same as Eq. (4.8). For simplicity, we set $r_h = 1$ throughout the following. To illustrate the numerical results, we show the holographic measures as functions of the rotation angle for different values of the anisotropy parameter in Figs. 12 and 13.

The left panel in Fig. 12 shows the turning point of the RT hypersurface for $\ell = 1$. Clearly, increasing the anisotropy, the RT hypersurfaces reach deeper into the bulk, thus they carry more information about the geometry. The right panel illustrates the finite part of the HEE which is an increasing function of a. Figure 13 shows the HMI and reflected entropy for specific values of ℓ and h. Although the reflected entropy increases with the anisotropy parameter for all values of the rotation angle, HMI is not a monotonic function of a. Moreover, at $\beta = \pi/2$ the HMI becomes maximum where the reflected entropy develops a minimum. Interestingly, while both HMI and reflected entropy are measures of total correlation between subregions, they do not behave in the same manner in this anisotropic boundary state. This behavior contrast with the results depicted in Fig. 10, where these measures behave in the same manner in a nonconformal boundary theory. We do not fully understand what is the reason for this behavior and leave it for future study.

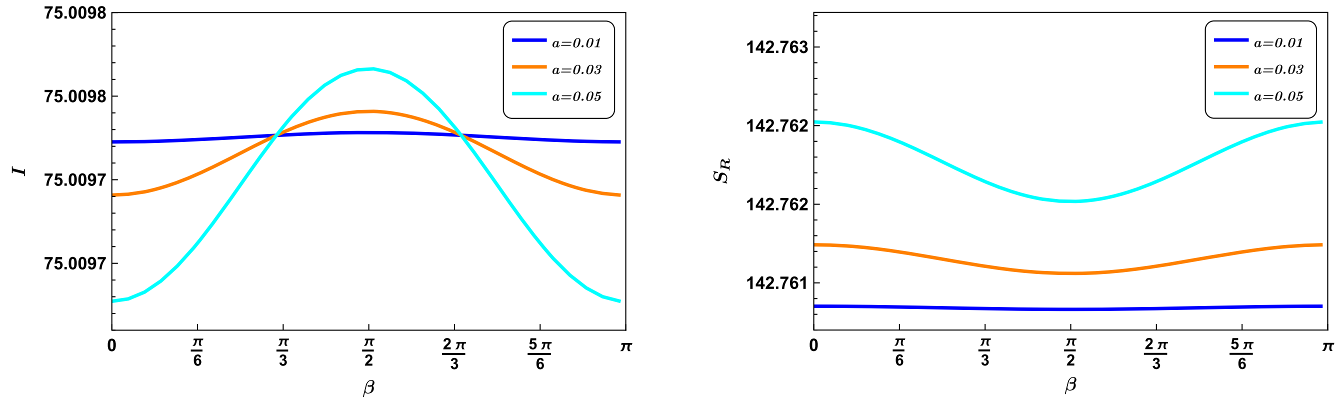

FIG. 13. HMI (left) and reflected entropy (right) as functions of β for $\ell = 0.1, h = 0.05, r_h = 1$ and different values of a.

V. LIFSHITZ-LIKE ANISOTROPIC MODELS

In this section we extend our studies to a specific geometry with anisotropic Lifshitz scale invariance first studied in [65]. This geometry is a type IIB supergravity solution and generated by intersections of D3 and D7 branes. The corresponding metric is given by

$$ds^2 = \frac{\tilde{R}^2}{r^2}\left(-f(r)dt^2 + \frac{dr^2}{f(r)} + dx^2 + dy^2 + r^{\frac{2}{3}}dz^2\right),$$
$$f(r) = 1 - \mu r^{\frac{11}{3}}, \tag{5.1}$$

where $\tilde{R}^2 = \frac{11}{12}R^2$ is the curvature radius of the spacetime. Further, μ gives the mass parameter of the black brane. This geometry is dual to a nonrelativistic boundary theory with the following expressions for temperature and energy density, respectively

$$T = \frac{11}{12\pi}\mu^{\frac{3}{11}}, \qquad \varepsilon = \frac{\tilde{R}^3}{6\pi G_N}\mu. \tag{5.2}$$

We see that for $\mu = 0$ metric (5.1) is invariant under an anisotropic scaling transformation $(t, r, x, y, z) \to (\lambda t, \lambda r, \lambda x, \lambda y, \lambda^{2/3} z)$ and thus can be regarded as a gravity dual of Lifshitz-like fixed point with dynamical exponent $\xi = \frac{3}{2}$. Let us recall that different aspects of holographic probes including viscosities and HEE in this model have been studied in [65]. Note that in this geometry, the strength of anisotropy between spatial directions is fixed, thus we only study the β-dependence of reflected entropy. In comparing the above background with metric (2.1), we should identify

$$G_1(r) = G_2(r) = H(r) = 1, \qquad G_3(r) = r^{\frac{2}{3}}. \tag{5.3}$$

The corresponding expression for HEE and reflected entropy can be obtained using Eqs. (2.6) and (2.7) and the above identifications. Before examining the full β-dependence of correlation measures, we would like to study the structure of divergent terms. Notice that because the metric (5.1) is not asymptotically AdS, the corresponding divergent terms that appear in HEE are more complicated. A straightforward calculation for $\beta > 0$, yields the following[2]

$$S_{\text{div}} = \frac{L^2 \sin\beta}{4G_N}\left(\frac{1}{\epsilon^2} + \frac{3\cot^2\beta}{4\epsilon^{4/3}} - \frac{3\cot^4\beta}{8\epsilon^{2/3}} - \frac{\cot^6\beta}{8}\log\epsilon\right). \tag{5.4}$$

Again, we see that a new universal logarithmic term appears, whose coefficient depends on the rotation angle.

Unfortunately, it is not possible to find the behavior of the reflected entropy analytically for general β. In the following, we present a combination of numerical and analytic results on the behavior of correlation measures for strip shaped boundary subregions. First, we provide a numerical analysis and examine the various properties of reflected entropy as a function of β. Next, we will show that at zero temperature and for specific values of the rotation angle, $\Sigma_{A\cup B}$ is a geodesic whose length can be expressed analytically in closed form, which enables us to directly extract its scaling behavior as a function of h and ℓ. We also carry out a perturbative analysis to compute low temperature corrections to reflected entropy at leading order.

A. Numerical results

In Fig. 14 we show the turning point and the finite part of HEE as functions of ℓ for several values of the rotation angle. In the figure, the dashed curves represent the finite temperature results and the solid curves correspond to $T = 0$ case. According to the left panel, for zero temperature case, at $\ell_c \sim 1.15$ different curves coincide and the location of the turning point is independent of β. Further, we note that for small subregions, i.e., $\ell < \ell_c$, the turning point decreases in anisotropic case compared to its AdS value which means that the bulk potential due to the anisotropy pushes the RT hypersurface toward the boundary. This behavior is enhanced by increasing the rotation angle from 0 to $\frac{\pi}{2}$. Moreover, from the right panel we see

[2]For $\beta = 0$ we have $S_{\text{div}} \sim \epsilon^{-5/3}$.

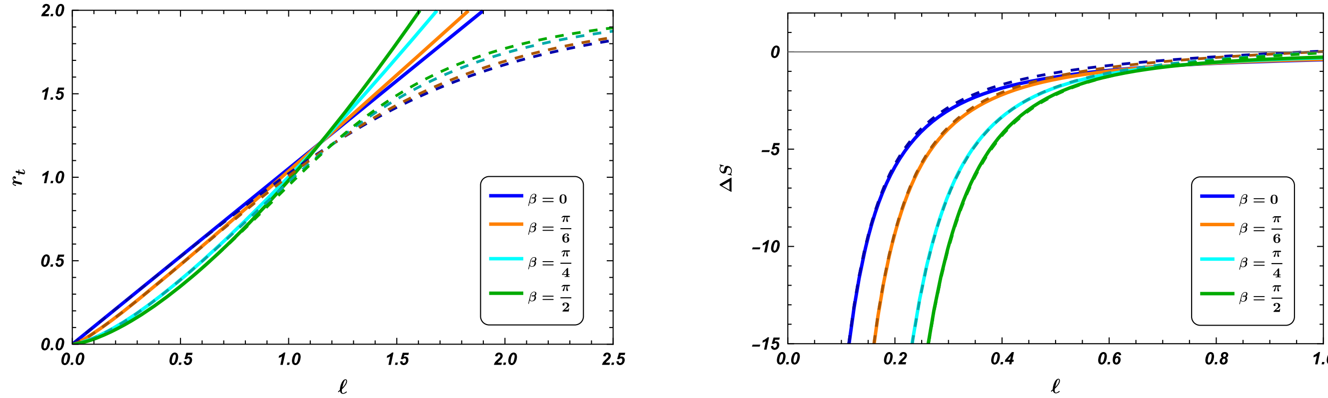

FIG. 14. The turning point of the RT hypersurface (left) and HEE (right) as functions of ℓ for different values of the rotation angle. The dashed curves represent the finite temperature results and the solid curves correspond to $T = 0$ case. Here we set $\mu = 0.079$ for left figure and $\mu = 1$ for right figure.

that for small subregions the finite part of the HEE is a monotonically decreasing function of β.

Figure 15 shows the HMI and reflected entropy as functions of $\frac{h}{\ell}$ for different values of β. Let us make a number of observations about these numerical results. First, we note that both HMI and reflected entropy are monotonically increasing functions of β. Next, the phase transition of the reflected entropy happens at larger separations between the subregions comparing to $\beta = 0$ case. Hence regarding the reflected entropy as a measure of total correlation between the subregions, we see that decreasing the rotation angle promote disentangling between them. Further, turning on the temperature, the phase transition of reflected entropy happens at smaller separations between the two subregions comparing to $T = 0$ case. Thus the thermal excitations decrease the total correlation between the subregions as expected.

B. Perturbative treatment

In this subsection, we present two specific examples in which we compute perturbatively the expression for the reflected entropy and other correlation measures. These two examples correspond to $\beta = 0$ and $\beta = \frac{\pi}{2}$ where due to the reflection symmetry, the profile of $\Sigma_{A\cup B}$ can be found exactly at zero temperature. Using this result, we can evaluate the thermal corrections to reflected entropy at low temperature.

1. $\beta = 0$

In this case, the width of the entangling region lies along the anisotropic direction. In order to investigate the low temperature behavior of reflected entropy, we insert Eq. (5.3) in Eqs. (2.6) and (2.7) and expand the resultant expressions in $hT \ll \ell T \ll 1$ limit which corresponds to $r_d \ll r_u \ll \mu^{-\frac{3}{11}}$. Hence, the corresponding turning points are close to the boundary. It is straightforward to evaluate the leading order correction with the result

$$\ell = r_t\left(c + \frac{3\sqrt{\pi}\Gamma(\frac{11}{8})}{14\Gamma(\frac{7}{8})}\mu r_t^{11/3}\right), \tag{5.5}$$

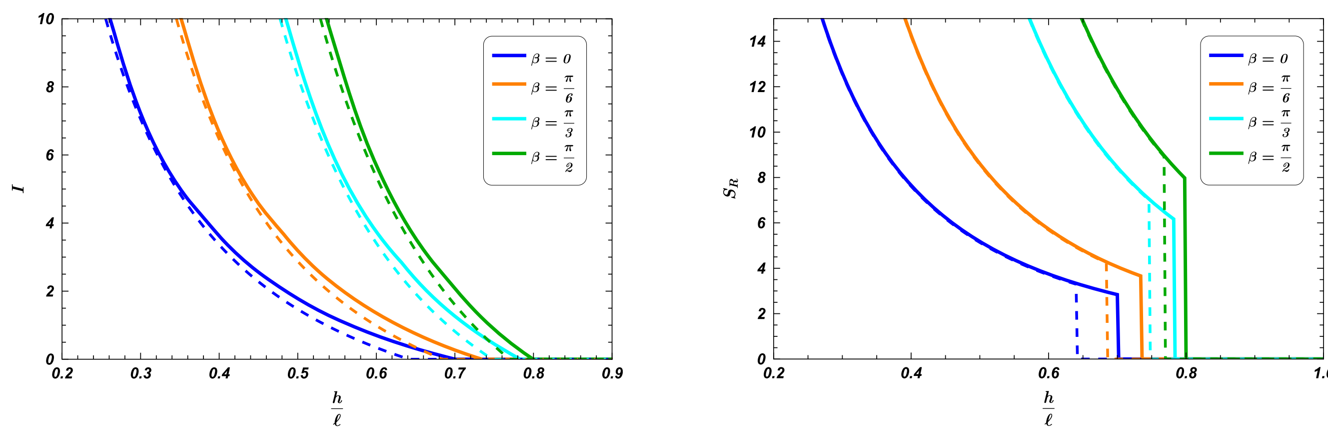

FIG. 15. HMI (left) and reflected entropy (right) as functions of $\frac{h}{\ell}$ for different values of β.Here we set $\mu = 1$.

where $c = \frac{2\sqrt{\pi}\Gamma(\frac{11}{16})}{\Gamma(\frac{3}{16})} > 0$. Inverting the above equation, we can represent the turning point as a function of ℓ

$$r_t = \frac{\ell}{c}\left(1 - \frac{3\sqrt{\pi}\Gamma(\frac{11}{8})}{14c^{14/3}\Gamma(\frac{7}{8})}\mu\ell^{\frac{11}{3}}\right). \qquad (5.6)$$

That is, increasing the temperature, the turning point of the RT hypersurface decreases. In this limit, the leading order behavior of HEE reduces to

$$S = \frac{\tilde{R}^3L^2}{2G_N}\frac{3}{5}\left(\frac{1}{\epsilon^{\frac{5}{3}}} - \frac{c}{2r_t^{\frac{5}{3}}} + \frac{5\sqrt{\pi}}{12}\frac{\Gamma(\frac{11}{8})}{\Gamma(\frac{7}{8})}\mu r_t^2\right). \qquad (5.7)$$

Now we would like to recast this result in terms of boundary quantities. We do so by combining Eqs. (5.6) and (5.7) which allow us to translate the first order correction of HEE to the form

$$\Delta S \equiv S - S_{\rm vac} = \tilde{c}L^2\ell^2\varepsilon, \qquad (5.8)$$

where $S_{\rm vac}$ is the vacuum contribution given by $S_{\rm vac} = \frac{3\tilde{R}^3L^2}{10G_N}(\frac{1}{\epsilon^{\frac{5}{3}}} - \frac{c^{\frac{8}{3}}}{2\ell^{\frac{5}{3}}})$ and $\tilde{c} = \frac{9\pi^{3/2}}{56c^2}\frac{\Gamma(\frac{3}{8})}{\Gamma(\frac{7}{8})}$. Note that $\tilde{c} > 0$ and hence thermal excitations increase the HEE as expected. These results allow us to find the variation of HMI as follows

$$\Delta I \equiv I - I_{\rm vac} = -2\tilde{c}L^2(\ell + h)^2\varepsilon, \qquad (5.9)$$

where $I_{\rm vac}$ is the vacuum contribution given by $I_{\rm vac} = -\frac{3\tilde{R}^3L^2c^{\frac{8}{3}}}{20G_N}(\frac{2}{\ell^{\frac{5}{3}}} - \frac{1}{h^{\frac{5}{3}}} - \frac{1}{(2\ell+h)^{\frac{5}{3}}})$. The minus sign shows that the thermal excitations decrease the HMI and hence reduce the total correlation between the subregions. Finally, we turn to the thermal corrections to the reflected entropy. It is straightforward to carry out the perturbative analysis and we find that

$$S_R = \frac{3\tilde{R}^3L^2}{10G_N}\left(\frac{1}{r_d^{\frac{5}{3}}} - \frac{1}{r_u^{\frac{5}{3}}}\right) + \frac{\tilde{R}^3L^2}{8G_N}\mu(r_u^2 - r_d^2). \qquad (5.10)$$

Now using Eq. (5.6) the leading contribution becomes

$$\Delta S_R \equiv S_R - S_{R\,\rm vac} = -\mathcal{C}L^2\ell(\ell + h)\varepsilon, \qquad (5.11)$$

where $S_{R\rm vac}$. is the vacuum contribution given by $S_{R\rm vac} = \frac{3\tilde{R}^3L^2c^{\frac{5}{3}}}{10G_N}(\frac{1}{h^{\frac{5}{3}}} - \frac{1}{(2\ell+h)^{\frac{5}{3}}})$ and $\mathcal{C} = \frac{3\pi}{c^2}(\frac{6\sqrt{\pi}}{7c}\frac{\Gamma(\frac{11}{8})}{\Gamma(\frac{7}{8})} - 1)$. We note again that this contribution is negative and hence the finite temperature corrections decrease the reflected entropy. Regarding this quantity as a measure of total correlation between the two subregions, we see that thermal excitations promote disentangling between them. These results are consistent with the previously numerical results illustrated in Fig. 15.

2. $\beta = \pi/2$

The analysis follows similarly to the previous case, with the obvious replacement of the rotation angle. Hence, we just report the final results in what follows. At leading order, the variation of HEE becomes

$$\Delta S \equiv S - S^{\pi/2}_{\rm vac} = L^2\tilde{c}\ell^{\frac{5}{2}}\varepsilon,$$

where $\tilde{c} = \frac{36\pi^{3/2}\Gamma(\frac{21}{16})}{65\Gamma(\frac{13}{16})}(\frac{2}{3c})^{5/2}$, $c = \frac{2\sqrt{\pi}\Gamma(\frac{5}{8})}{\Gamma(\frac{1}{8})}$ and $S^{\pi/2}_{\rm vac}$ is the vacuum contribution in $\beta = \frac{\pi}{2}$ given by

$$S^{\pi/2}_{\rm vac} = \frac{\tilde{R}^3L^2}{8G_N}\left(\frac{2}{\epsilon^2} - \frac{c^4}{(\frac{2\ell}{3})^3}\right). \qquad (5.12)$$

Equipped with the above result we can compute HMI as follows

$$\Delta I \equiv I - I^{\pi/2}_{\rm vac} = -L^2\tilde{c}((2\ell + h)^{5/2} - 2\ell^{5/2} + h^{5/2})\varepsilon, \qquad (5.13)$$

where $I^{\pi/2}_{\rm vac}$ is the vacuum contribution in $\beta = \frac{\pi}{2}$ given by

$$I^{\pi/2}_{\rm vac} = -\frac{\tilde{R}^3L^2}{12G}\left(\frac{3\sqrt{\pi}\Gamma(\frac{5}{8})}{\Gamma(\frac{1}{8})}\right)^4\left(\frac{2}{\ell^3} - \frac{1}{h^3} - \frac{1}{(2\ell + h)^3}\right). \qquad (5.14)$$

Finally, the variation of reflected entropy becomes

$$\Delta S_R \equiv S_R - S^{\pi/2}_{R\,\rm vac} = -\tilde{\mathcal{C}}L^2((h + 2l)^{5/2} - h^{5/2})\varepsilon, \qquad (5.15)$$

where $\tilde{\mathcal{C}} = \frac{9\pi}{10c^{5/2}}(\frac{2}{3})^{5/2}(\frac{10\sqrt{\pi}\Gamma(\frac{21}{16})}{13c\Gamma(\frac{13}{16})} - 1)$ and $S^{\pi/2}_{R\,\rm vac} = \frac{27\tilde{R}^3L^2}{32G_N} \times c^3(\frac{1}{h^3} - \frac{1}{(2\ell+h)^3})$. Again, these agree with the results shown in Fig. 15, where we see that thermal excitations promote disentangling between the subregions.

VI. CONCLUSIONS AND DISCUSSIONS

In this paper, we explored the behavior of reflected entropy in certain nonrelativistic geometries dual to anisotropic boundary systems. We used the holographic proposal for computing this quantity which states that reflected entropy is proportional to the minimal cross-sectional area of the entanglement wedge, as in Eq. (1.7). Specifically, we have focused on symmetric boundary configurations consisting of two disjoint strips with equal width, which is the simplest case to utilize the holographic proposal to compute the correlation measures. In principle though, we expect that the qualitative features of our results are independent of the specific configuration. Although some of the intermediate steps may differ, we expect that the qualitative features of our results are hold for non symmetric

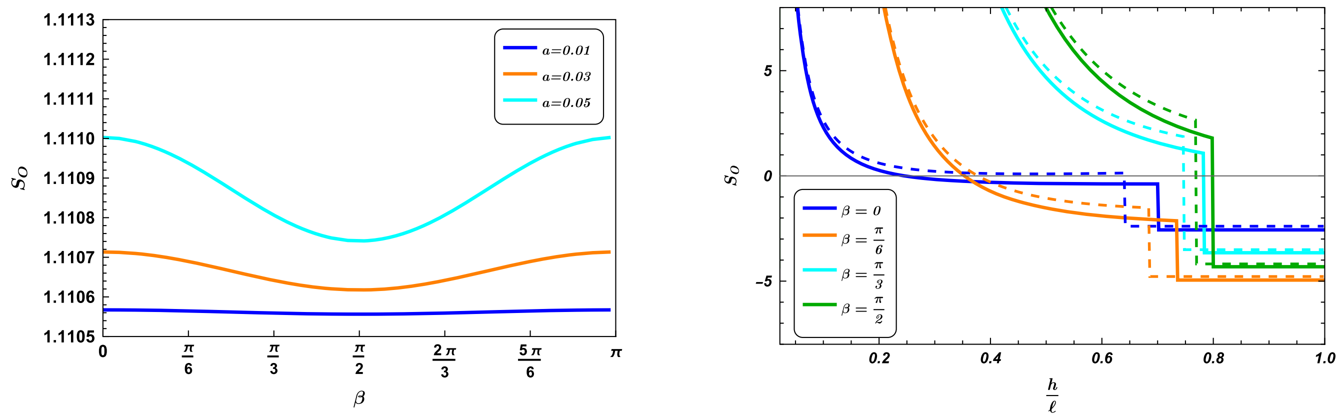

FIG. 16. Left: odd entropy as a function of β for different values of the anisotropy parameter for model discussed in Sec. IV A. Right: odd entropy as a function of $\frac{h}{\ell}$ for different values of β for model discussed in Sec. V. The dashed curves represent the finite temperature results and the solid curves correspond to $T = 0$ case.

configurations. In addition to numerical analysis, in specific anisotropic backgrounds we evaluated the leading order corrections to holographic correlation measures analytically. We also compared the behavior of reflected entropy to other correlation measures including HEE and HMI.

Our analysis in this paper focused mainly on the effect of anisotropy on reflected entropy and other correlation measures. Generally, the additional contributions due to the anisotropy parameter or rotation angle to this quantity do not have a definite sign. For example, based on our results in Sec. III, we found that S_R is an increasing function of the anisotropy parameter, i.e., ν, in a specific range of rotation angle such that it develops a maximum at $\beta = \pi/2$. Interestingly, at the same value of the rotation angle, the critical separation between the subregions is a monotonically increasing function of ν and hence the correlation between the subregions becomes stronger (see Fig. 5). On the other hand, both our analytic calculations and numerical analysis in Sec. IV A gave evidence that the reflected entropy has a minimum at $\beta = \pi/2$ and is a monotonically decreasing function of the anisotropy parameter [see the panel in Fig. 10 and Eq. (4.21)].

In addition to these differences, at a qualitative level, all of the cases considered in this work had a number of common features in all cases examples. First, the variation of HMI and reflected entropy has the sign due to presence of the anisotropy. Regarding these quantities as measures of total correlation between the subregions, this behavior seems reasonable. Although, this result is different from what happens for the HEE where the variation flips its sign. This feature precisely matches with the previous results of [56,66,67]. Another key feature which was observed here was the appearance of a new universal logarithmic term in HEE whose coefficient depends on the anisotropy parameter and the rotation angle. Roughly, we can think of this universal term as characterizing when the isotropy is broken in the underlying boundary theory. Similarly, as shown in [55], if instead we choose a background which breaks the translation invariance the structure of the universal terms of HEE is modified. This feature is entirely expected given our experiences from HEE in other backgrounds with broken symmetries, e.g., see [64].

Recall that some holographic proposals consider other candidates for the mixed state correlation measures dual to EWCS. For example, based on [9], in holographic theories the odd entropy can be written in terms of the reflected entropy as follows

$$S_O(A, B) = \frac{S_R(A, B)}{2} + S(A \cup B).$$

Using this expression we can find the odd entropy using our previous results for reflected entropy in different anisotropic boundary systems. In Fig. 16 we plot this measure in two of our models in Secs. IV A and V. The left panel shows that in the nonconformal boundary theory, odd entropy is an increasing function of the anisotropy parameter and hence the correlation between the subregions becomes more pronounced. Clearly the β dependence of this measure is similar to HMI and reflected entropy as expected (see Fig. 10). In the right panel we plot odd entropy as a function of $\frac{h}{\ell}$ for different values of β in the Lifshitz-like anisotropic background. The dashed curves represent the finite temperature results and the solid curves correspond to the zero temperature case. Regarding the odd entropy as a measure of correlation, we see that decreasing the rotation angle promote disentangling between the subregions. Let us mention that the qualitative features of the odd entropy in other anisotropic models are similar, thus we neglect to present them.

We can extend this study to different interesting directions. In this paper we focused on symmetric configuration for the boundary entangling regions which significantly simplifies the computation of the reflected entropy. It is also interesting to look at more complicated setups where the widths of the strips are different, using the method first introduced in [68]. Another interesting question is if either of these behaviors can be extracted from field theory calculations of reflected entropy using the techniques developed in [35,36]. We plan to explore some of these directions in the near future.

ACKNOWLEDGMENTS

We are very grateful to Mohammad Hasan Vahidinia for careful reading of the manuscript and his valuable comments. We would also like to thank the referee for her/his useful comments.

[1] S. Ryu and T. Takayanagi, Holographic Derivation of Entanglement Entropy from AdS/CFT, Phys. Rev. Lett. **96**, 181602 (2006).

[2] A. R. Brown, D. A. Roberts, L. Susskind, B. Swingle, and Y. Zhao, Holographic Complexity Equals Bulk Action?, Phys. Rev. Lett. **116**, 191301 (2016).

[3] H. Casini and M. Huerta, Entanglement entropy in free quantum field theory, J. Phys. A **42**, 504007 (2009).

[4] T. Nishioka, Entanglement entropy: Holography and renormalization group, Rev. Mod. Phys. **90**, 035007 (2018).

[5] T. Nishioka, S. Ryu, and T. Takayanagi, Holographic entanglement entropy: An overview, J. Phys. A **42**, 504008 (2009).

[6] M. Rangamani and T. Takayanagi, Holographic entanglement entropy, Lect. Notes Phys. **931**, 1 (2017).

[7] M. B. Plenio, Logarithmic Negativity: A Full Entanglement Monotone That is Not Convex, Phys. Rev. Lett. **95**, 090503 (2005).

[8] B. M. Terhal, M. Horodecki, D. W. Leung, and D. P. DiVincenzo, The entanglement of purification, J. Math. Phys. (N.Y.) **43**, 4286 (2002).

[9] K. Tamaoka, Entanglement Wedge Cross Section from the Dual Density Matrix, Phys. Rev. Lett. **122**, 141601 (2019).

[10] S. Dutta and T. Faulkner, A canonical purification for the entanglement wedge cross-section, J. High Energy Phys. 03 (2021) 178.

[11] Y. Kusuki, J. Kudler-Flam, and S. Ryu, Derivation of Holographic Negativity in AdS_3/CFT_2, Phys. Rev. Lett. **123**, 131603 (2019).

[12] T. Takayanagi and K. Umemoto, Entanglement of purification through holographic duality, Nat. Phys. **14**, 573 (2018).

[13] P. Nguyen, T. Devakul, M. G. Halbasch, M. P. Zaletel, and B. Swingle, Entanglement of purification: From spin chains to holography, J. High Energy Phys. 01 (2018) 098.

[14] H. Hirai, K. Tamaoka, and T. Yokoya, Towards entanglement of purification for conformal field theories, Prog. Theor. Exp. Phys. **2018**, 063B03 (2018).

[15] K. Babaei Velni, M. R. Mohammadi Mozaffar, and M. H. Vahidinia, Some aspects of entanglement wedge cross-section, J. High Energy Phys. 05 (2019) 200.

[16] N. Jokela and A. Pönni, Notes on entanglement wedge cross sections, J. High Energy Phys. 07 (2019) 087.

[17] K. Umemoto, Quantum and classical correlations inside the entanglement wedge, Phys. Rev. D **100**, 126021 (2019).

[18] C. Akers and P. Rath, Entanglement wedge cross sections require tripartite entanglement, J. High Energy Phys. 04 (2020) 208.

[19] B. Amrahi, M. Ali-Akbari, and M. Asadi, Holographic entanglement of purification near a critical point, Eur. Phys. J. C **80**, 1152 (2020).

[20] S. Chakrabortty, S. Pant, and K. Sil, Effect of back reaction on entanglement and subregion volume complexity in strongly coupled plasma, J. High Energy Phys. 06 (2020) 061.

[21] A. Saha and S. Gangopadhyay, Holographic study of entanglement and complexity for mixed states, Phys. Rev. D **103**, 086002 (2021).

[22] R. Q. Yang, C. Y. Zhang, and W. M. Li, Holographic entanglement of purification for thermofield double states and thermal quench, J. High Energy Phys. 01 (2019) 114.

[23] Y. Kusuki and K. Tamaoka, Dynamics of entanglement wedge cross section from conformal field theories, Phys. Lett. B **814**, 136105 (2021).

[24] H. S. Jeong, K. Y. Kim, and M. Nishida, Reflected entropy and entanglement wedge cross section with the first order correction, J. High Energy Phys. 12 (2019) 170.

[25] J. Kudler-Flam, Y. Kusuki, and S. Ryu, Correlation measures and the entanglement wedge cross-section after quantum quenches in two-dimensional conformal field theories, J. High Energy Phys. 04 (2020) 074.

[26] K. Babaei Velni, M. R. Mohammadi Mozaffar, and M. H. Vahidinia, Evolution of entanglement wedge cross section following a global quench, J. High Energy Phys. 08 (2020) 129.

[27] M. Moosa, Time dependence of reflected entropy in conformal field theory, J. High Energy Phys. 05 (2020) 082.

[28] J. Boruch, Entanglement wedge cross-section in shock wave geometries, J. High Energy Phys. 07 (2020) 208.

[29] S. Khoeini-Moghaddam, F. Omidi, and C. Paul, Aspects of hyperscaling violating geometries at finite cutoff, J. High Energy Phys. 02 (2021) 121.

[30] D. Basu, H. Parihar, V. Raj, and G. Sengupta, Entanglement negativity, reflected entropy, and anomalous gravitation, Phys. Rev. D **105**, 086013 (2022); **105**, 129902(E) (2022).

[31] J. K. Basak, H. Chourasiya, V. Raj, and G. Sengupta, Reflected entropy in Galilean conformal field theories and flat holography, arXiv:2202.01201.

[32] Y. Kusuki and K. Tamaoka, Entanglement wedge cross section from CFT: Dynamics of local operator quench, J. High Energy Phys. 02 (**2020**) 017.

[33] A. Mollabashi and K. Tamaoka, A field theory study of entanglement wedge cross section: Odd entropy, J. High Energy Phys. 08 (2020) 078.

[34] C. Berthiere, H. Chen, Y. Liu, and B. Chen, Topological reflected entropy in Chern-Simons theories, Phys. Rev. B **103**, 035149 (2021).

[35] P. Bueno and H. Casini, Reflected entropy for free scalars, J. High Energy Phys. 11 (**2020**) 148.

[36] H. A. Camargo, L. Hackl, M. P. Heller, A. Jahn, and B. Windt, Long-Distance Entanglement of Purification and Reflected Entropy in Conformal Field Theory, Phys. Rev. Lett. **127**, 141604 (2021).

[37] Q. Wen, Balanced partial entanglement and the entanglement wedge cross section, J. High Energy Phys. 04 (2021) 301.

[38] P. Hayden, O. Parrikar, and J. Sorce, The Markov gap for geometric reflected entropy, J. High Energy Phys. 10 (2021) 047.

[39] C. Akers, T. Faulkner, S. Lin, and P. Rath, Reflected entropy in random tensor networks, J. High Energy Phys. 05 (2022) 162.

[40] P. Bueno and H. Casini, Reflected entropy, symmetries and free fermions, J. High Energy Phys. 05 (2020) 103.

[41] H. A. Camargo, P. Nandy, Q. Wen, and H. Zhong, Balanced partial entanglement and mixed state correlations, SciPost Phys. **12**, 137 (2022).

[42] D. Mateos and D. Trancanelli, Thermodynamics and instabilities of a strongly coupled anisotropic plasma, J. High Energy Phys. 07 (2011) 054.

[43] R. Rougemont, R. Critelli, and J. Noronha, Holographic calculation of the QCD crossover temperature in a magnetic field, Phys. Rev. D **93**, 045013 (2016).

[44] A. Rebhan and D. Steineder, Violation of the Holographic Viscosity Bound in a Strongly Coupled Anisotropic Plasma, Phys. Rev. Lett. **108**, 021601 (2012).

[45] D. Mateos and D. Trancanelli, The Anisotropic $N = 4$ Super Yang-Mills Plasma and its Instabilities, Phys. Rev. Lett. **107**, 101601 (2011).

[46] D. Giataganas, Probing strongly coupled anisotropic plasma, J. High Energy Phys. 07 (2012) 031.

[47] M. Chernicoff, D. Fernandez, D. Mateos, and D. Trancanelli, Drag force in a strongly coupled anisotropic plasma, J. High Energy Phys. 08 (2012) 100.

[48] M. Ali-Akbari and H. Ebrahim, Chiral symmetry breaking: To probe anisotropy and magnetic field in quark-gluon plasma, Phys. Rev. D **89**, 065029 (2014).

[49] S. S. Pal, Anisotropic gravity solutions in AdS/CMT, arXiv:0901.0599.

[50] T. Azeyanagi, W. Li, and T. Takayanagi, On string theory duals of Lifshitz-like fixed points, J. High Energy Phys. 06 (2009) 084.

[51] K. Narayan, T. Takayanagi, and S. P. Trivedi, AdS plane waves and entanglement entropy, J. High Energy Phys. 04 (2013) 051.

[52] V. Jahnke, Delocalizing entanglement of anisotropic black branes, J. High Energy Phys. 01 (2018) 102.

[53] S. Mahapatra, Interplay between the holographic QCD phase diagram and mutual & *n*-partite information, J. High Energy Phys. 04 (2019) 137.

[54] I. Y. Aref'eva, A. Patrushev, and P. Slepov, Holographic entanglement entropy in anisotropic background with confinement-deconfinement phase transition, J. High Energy Phys. 07 (2020) 043.

[55] P. Jain and S. Mahapatra, Mixed state entanglement measures as probe for confinement, Phys. Rev. D **102**, 126022 (2020).

[56] M. Sahraei, M. J. Vasli, M. R. M. Mozaffar, and K. B. Velni, Entanglement wedge cross section in holographic excited states, J. High Energy Phys. 08 (2021) 038.

[57] I. Aref'eva and K. Rannu, Holographic anisotropic background with confinement-deconfinement phase transition, J. High Energy Phys. 05 (**2018**) 206.

[58] I. R. Klebanov, D. Kutasov, and A. Murugan, Entanglement as a probe of confinement, Nucl. Phys. **B796**, 274 (2008).

[59] S. S. Gubser and A. Nellore, Mimicking the QCD equation of state with a dual black hole, Phys. Rev. D **78**, 086007 (2008).

[60] S. S. Gubser, A. Nellore, S. S. Pufu, and F. D. Rocha, Thermodynamics and Bulk Viscosity of Approximate Black Hole Duals to Finite Temperature Quantum Chromodynamics, Phys. Rev. Lett. **101**, 131601 (2008).

[61] D. Giataganas, U. Gürsoy, and J. F. Pedraza, Strongly-Coupled Anisotropic Gauge Theories and Holography, Phys. Rev. Lett. **121**, 121601 (2018).

[62] U. Gursoy, E. Kiritsis, and F. Nitti, Exploring improved holographic theories for QCD: Part II, J. High Energy Phys. 02 (2008) 019.

[63] M. Ghasemi and S. Parvizi, Constraints on anisotropic RG flows from holographic entanglement entropy, Phys. Rev. D **104**, 086028 (2021).

[64] M. Reza Mohammadi Mozaffar, A. Mollabashi, and F. Omidi, Non-local probes in holographic theories with momentum relaxation, J. High Energy Phys. 10 (2016) 135.

[65] T. Azeyanagi, W. Li, and T. Takayanagi, On string theory duals of Lifshitz-like fixed points, J. High Energy Phys. 06 (2009) 084.

[66] D. D. Blanco, H. Casini, L. Y. Hung, and R. C. Myers, Relative entropy and holography, J. High Energy Phys. 08 (2013) 060.

[67] M. Alishahiha, M. R. Mohammadi Mozaffar, and M. R. Tanhayi, On the time evolution of holographic n-partite information, J. High Energy Phys. 09 (2015) 165.

[68] P. Liu, Y. Ling, C. Niu, and J. P. Wu, Entanglement of purification in holographic systems, J. High Energy Phys. 09 (2019) 071.